

Switching Rashba spin-splitting by reversing electric-field direction

San-Dong Guo¹, Jing-Xin Zhu¹, Hao-Tian Guo¹, Bing Wang², Guang-Zhao Wang³ and Yee-Sin Ang⁴

¹*School of Electronic Engineering, Xi'an University of Posts and Telecommunications, Xi'an 710121, China*

²*Institute for Computational Materials Science, School of Physics and Electronics, Henan University, 475004, Kaifeng, China*

³*Key Laboratory of Extraordinary Bond Engineering and Advanced Materials Technology of Chongqing, School of Electronic Information Engineering, Yangtze Normal University, Chongqing 408100, China and*

⁴*Science, Mathematics and Technology (SMT), Singapore University of Technology and Design (SUTD), 8 Somapah Road, Singapore 487372, Singapore*

The manipulation of the Rashba spin-splitting is crucial for the development of nanospintronic technology. Here, it is proposed that the Rashba spin-splitting can be turned on and off by reversing electric-field direction. By the first-principle calculations, our proposal is illustrated by a concrete example of Janus monolayer RbKNaBi. The designed RbKNaBi possesses dynamical, thermal and mechanical stability, and is a large-gap quantum spin Hall insulator (QSHI) with Rashba spin-splitting near the Fermi level. A small built-in electric field is predicted due to very small electronegativity difference between the bottom and top atoms, which is very key to switch Rashba spin-splitting through the experimentally available electric field intensity. Due to out-of-plane structural asymmetry, the Janus monolayer has distinctive behaviors by applying external electric field E with the same magnitude but different directions (z or $-z$). Our results reveal that the Rashba energy (E_R) and Rashba constant (α_R) are increased by the positive E , while a negative E suppresses the Rashba splitting to disappear, and then appears again. In a certain E region (0.15 V/Å to 0.25 V/Å), switching Rashba spin-splitting can be achieved by only reversing electric-field direction. Besides, the piezoelectric strain coefficients d_{11} and d_{31} (5.52 pm/V and -0.41 pm/V) are predicted, which are higher than or compared with those of many 2D materials. By piezoelectric effect, the strain can also be used to tune Rashba spin-splitting of RbKNaBi. In Janus RbKNaBi monolayer, the combination of piezoelectricity and Rashba spin-splitting with topological insulating phase is pregnant to promote the integration of fantastic physical phenomenons. Moreover, a possible spintronic device is proposed to realize the function of spintronic switch. Our proposed manipulation of the Rashba spin-splitting may make a special contribution to semiconductor spintronics.

Keywords: Electric field, Rashba spin-splitting, Piezoelectricity

Email:sandongyuwang@163.com

I. INTRODUCTION

Spintronics has attracted considerable attention, which can transmit information using spins rather than charges by manipulating the spin degree of freedom of electrons¹. The semiconductor spintronic devices are compatible with the integration technologies of conventional semiconductor nanoelectronic devices. Generating spin currents is necessary for semiconductor spintronic devices, which can be achieved by spin-orbit coupling (SOC)². The SOC-induced spin splitting exists in non-centrosymmetric structures, mainly including two types: the Rashba effect induced by the structure inversion asymmetry^{3,4} and the Dresselhaus effect induced by the bulk inversion asymmetry². Here, we concentrate on Rashba spin-splitting in two-dimensional (2D) materials.

When an electron moves across an electric field \vec{E} , it experiences an effective magnetic field $\vec{B}_{eff} \sim \vec{E} \times \vec{p}/mc^2$ in its rest-frame. The effective magnetic field can induce a momentum-dependent Zeeman energy $H_{SOC} \sim \mu_B(\vec{E} \times \vec{p}) \cdot \vec{\sigma}/mc^2$. In crystals, the electric field \vec{E} is the gradient of the crystal potential. For 2D Janus materials, there is a built-in electric field \vec{E} along the z ($\vec{E} = E_z \vec{z}$), and the spin degeneracy of the energy spectrum is lifted, which can be described by the Rashba Hamiltonian^{3,4}:

$$H_R = \frac{\alpha_R}{\hbar} (\vec{z} \times \vec{p}) \cdot \vec{\sigma} \quad (1)$$

where α_R is proportional to E . The spin splitting of the energy spectrum is called Rashba spin-splitting. The Rashba semiconductors have been predicted in many 2D Janus materials⁵⁻¹⁰

It is a natural idea to turn on and off Rashba spin-splitting through an external electric field. As shown **Figure 1** (a), a 2D Janus material with a built-in electric field E_b possesses Rashba spin-splitting. By applying an appropriate positive electric field E_p along z direction, the Rashba spin-splitting is enhanced. However, when the applied electric field is reversed ($\vec{E}_n = -\vec{E}_p$), the Rashba spin-splitting will disappear. In experiment, the external electric field can be as high as 0.3 V/Å¹¹. To accomplish our proposal practically, a 2D Janus material should meet these conditions: (1) there is a Rashba spin-splitting, and it's better to be at the Γ point; (2) the electronegativity difference between the bottom and top atoms is small, which will induce small built-in electric field; (3) there are heavy elements, which may produce observable Rashba spin-splitting and remedy for small built-in electric field.

The MoSSe is a representative 2D Janus material, which has been synthesized experimentally^{12,13}. However, the magnitude of the inherent electric field of MoSSe is 0.856 V/Å¹⁴, which is beyond the available experimental size of electric field (0.3 V/Å)¹¹. It has been proved that the Rashba spin-splitting of MoSSe still maintains

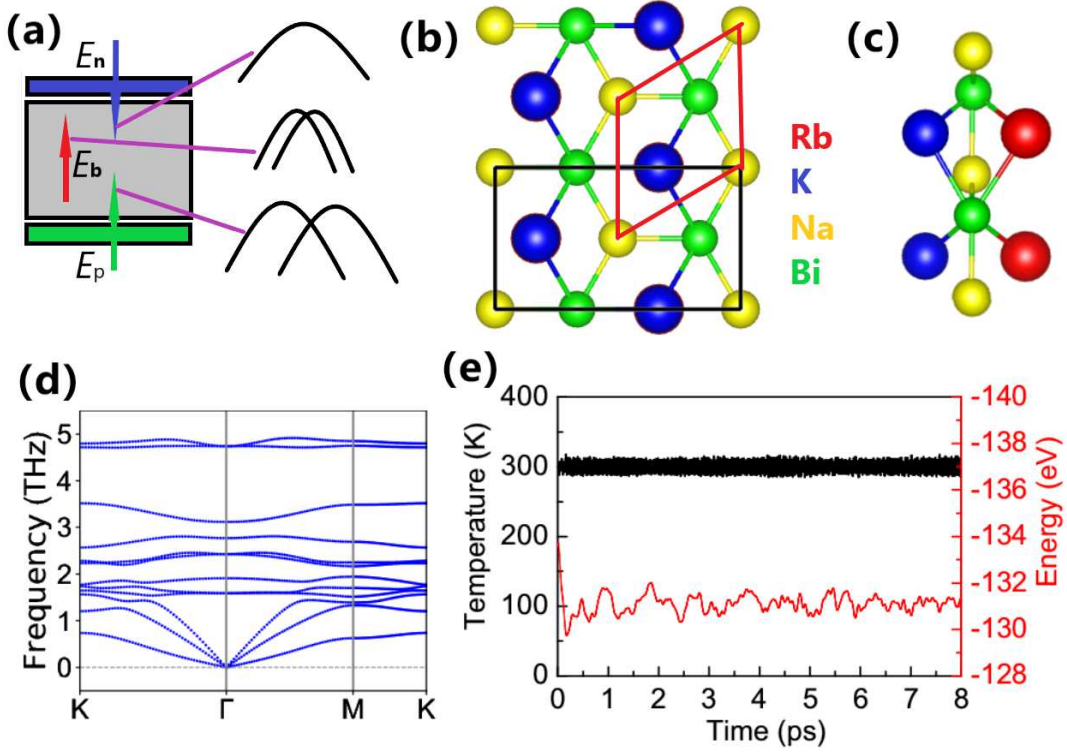


FIG. 1. (Color online)(a):a 2D Janus material with a built-in electric field E_b possesses Rashba spin-splitting. When an appropriate positive electric field E_p along z direction is applied, the Rashba spin-splitting is enhanced. However, the applied electric field is reversed ($\vec{E}_n = -\vec{E}_p$), and the Rashba spin-splitting will disappear. For Janus monolayer RbKNaBi, (b) top view and (c) side view of crystal structure, and the primitive cell (rectangle supercell) is marked by red (black) frames; (d):The phonon band dispersions; (e):The temperature and total energy fluctuations as a function of simulation time at 300 K.

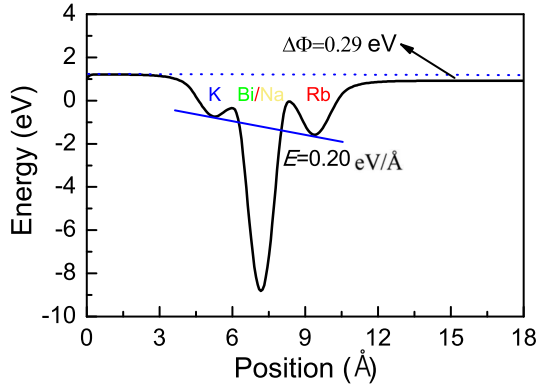


FIG. 2. (Color online)For RbKNaBi monolayer, the planar averaged electrostatic potential energy variation along z . $\Delta\Phi$ is the potential energy difference across the layer. E means built-in electric field.

by applying the external electric field of -0.5 V/\AA^{15} . Recently, the large-gap QSHIs K_2NaBi and Rb_2NaBi monolayers are predicted with Na_3Bi -like crystal structure¹⁶, and they have sandwich structures. The Na atoms are connected with Bi atoms forming a graphene-like sheet in the ab plane, while the K/Rb atoms are above and below NaBi layer. In this work, we construct a Janus

RbKNaBi material by replacing one of two K/Rb layers with Rb/K atoms in monolayer $\text{K}_2\text{NaBi/Rb}_2\text{NaBi}$. The artificial RbKNaBi meets the three conditions mentioned above to switch Rashba spin-splitting by reversing electric-field direction. By the first-principle calculations, our idea is illustrated in Janus monolayer RbKNaBi as a QSHI. It is found that the increasing positive external electric field can enhance Rashba energy (E_R) and Rashba constant (α_R). However, the increasing negative external electric field firstly quenches Rashba spin-splitting, and then recover it again. In a certain electric field region, simply reversing electric-field direction can switch Rashba spin-splitting. Finally, the piezoelectric properties of RbKNaBi are studied, and the strain-induced electric field by piezoelectric effect can be used to tune Rashba spin-splitting of RbKNaBi. Our proposed manipulation of the Rashba spin-splitting can be used for future spintronic devices.

The rest of the paper is organized as follows. In the next section, we shall give our computational details and methods. In the next few sections, we shall present crystal Structure and structural Stability, electronic structures along with electric field effects and piezoelectric properties of Janus monolayer RbKNaBi. Finally, we shall give our discussion and conclusion.

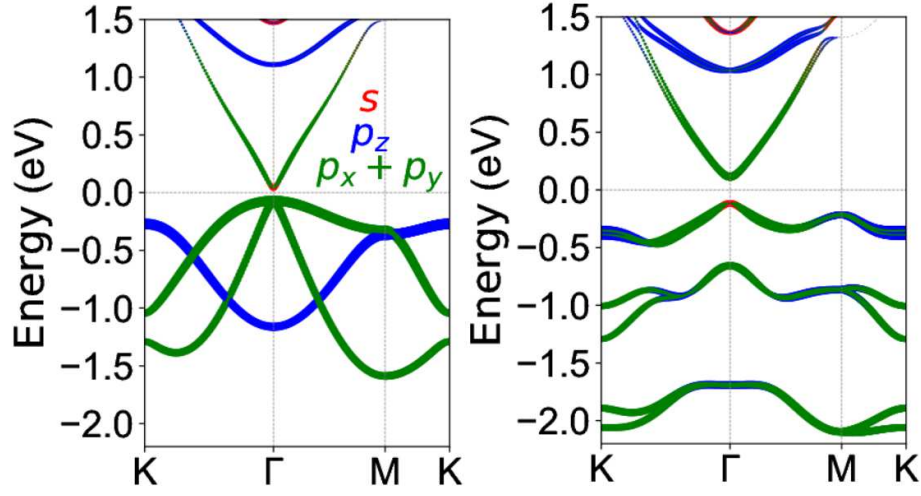


FIG. 3. (Color online) The Bi- s , $p_x + p_y$ and p_z projected band structures of Janus monolayer RbKNaBi from GGA and GGA+SOC, respectively. The band inversion induced by SOC can be clearly observed at the Γ point.

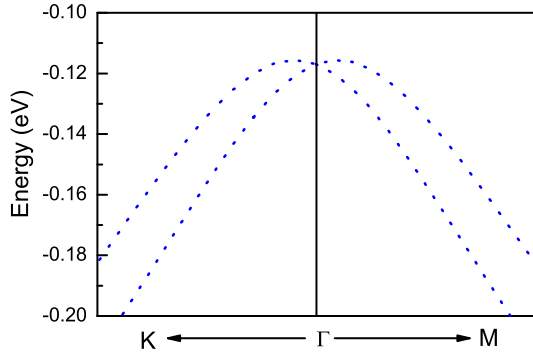


FIG. 4. (Color online) The enlarged valence bands centered at the Γ point near the Fermi level for RbKNaBi.

II. COMPUTATIONAL DETAIL

Within density functional theory (DFT)¹⁷, the first-principles calculations are carried out using the projected augmented wave (PAW) method with a kinetic cutoff energy of 500 eV, as implemented in the Vienna ab initio simulation package (VASP)^{18–20}. The generalized gradient approximation (GGA) of Perdew, Burke and Ernzerhof²¹ is adopted as the exchange-correlation potential. The total energy convergence criterion of 10^{-8} eV and residual force of less than $0.0001 \text{ eV} \cdot \text{\AA}^{-1}$ on each atom are set to obtain accurate results. A vacuum spacing of larger than 16 \AA along the z direction is included to avoid interactions between two neighboring images. The SOC is incorporated for band structure calculations.

The phonon dispersions are performed using a finite difference approach with a supercell of $5 \times 5 \times 1$, as implemented in Phonopy code²². We calculate the elastic stiffness tensor C_{ij} and piezoelectric stress coefficients e_{ij} by using strain-stress relationship (SSR) and density functional perturbation theory (DFPT) method²³,

respectively. The 2D elastic coefficients C_{ij}^{2D} and piezoelectric stress coefficients e_{ij}^{2D} have been renormalized by the length of unit cell along z direction (L_z): $C_{ij}^{2D} = L_z C_{ij}^{3D}$ and $e_{ij}^{2D} = L_z e_{ij}^{3D}$. A Γ -centered $12 \times 12 \times 1$ k-point meshes in the Brillouin zone (BZ) is adopted to calculate C_{ij} and electronic structures, and a $8 \times 12 \times 1$ Monkhorst-Pack k-point meshes for e_{ij} . The WannierTools code²⁴ is used to investigate topological properties of RbKNaBi, based on the tight-binding Hamiltonians constructed from maximally localized Wannier functions, as implemented in Wannier90 code²⁵. The PYPROCAR code is used to obtain the constant energy contour plots of the spin texture²⁶.

III. CRYSTAL STRUCTURE AND STRUCTURAL STABILITY

As shown in Figure 1 (b) and (c), the RbKNaBi monolayer shares the honeycomb crystal with the space group of $P3m1$ (No.156). The Na, K and Rb atoms are all bonded to the surrounding three Bi atoms, and Na and Bi atoms form a layer, while K and Rb atoms form two more layers. The symmetry of RbKNaBi is lower than that of $\text{K}_2\text{NaBi}/\text{Rb}_2\text{NaBi}$ with the space group of $P\bar{6}m2$ (No.187). The RbKNaBi and $\text{K}_2\text{NaBi}/\text{Rb}_2\text{NaBi}$ all lack the spatial inversion symmetry. Besides, the RbKNaBi also lacks horizontal mirror symmetry, which will induce out-of-plane piezoelectricity and Rashba effect. The Janus monolayer RbKNaBi can be constructed by replacing one of two K/Rb layers with Rb/K atoms in monolayer $\text{K}_2\text{NaBi}/\text{Rb}_2\text{NaBi}$. The optimized lattice parameters a of RbKNaBi is 5.587 \AA , which is between ones of K_2NaBi (5.548 \AA) and Rb_2NaBi (5.629 \AA).

The phonon spectra, ab initio molecular dynamics (AIMD) simulations and elastic constants C_{ij} are calculated to confirm the stability of RbKNaBi. As shown

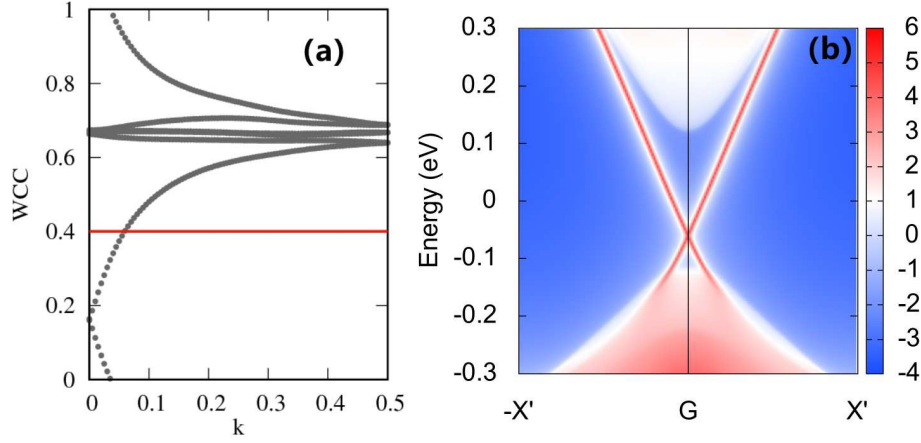


FIG. 5. (Color online) For RbKNaBi monolayer, (a): calculated WCC evolutions based on the GGA+SOC electronic structure, indicating a nontrivial Z_2 invariant ($Z_2=1$). (b): the projected edge spectra with a bulk electronic structure, showing a nontrivial metallic edge state.

in Figure 1 (d), no imaginary vibrational frequency can be observed, which clearly suggests that the RbKNaBi is dynamically stable. Moreover, both linear and flexural modes can be observed around the Γ point, which shares the general features of 2D materials^{27,28}. The AIMD simulation is performed by using the canonical (NVT) ensemble with a $4 \times 4 \times 1$ supercell at 300 K for 8 ps with a time step of 1 fs. As shown in Figure 1 (e), the total energy and temperature fluctuate in the simulation time, but the average energy and temperature remain almost invariant. The final atomic configuration shows no obvious distortion of the geometric structure after 8000 steps of AIMD simulation, which can allow returning to its initiating structure by optimizing this final configuration. These results indicate its thermal stability of RbKNaBi at room temperature.

Due to $P3m1$ symmetry, the 2D elastic tensor with using Voigt notation can be reduced into:

$$C = \begin{pmatrix} C_{11} & C_{12} & 0 \\ C_{12} & C_{11} & 0 \\ 0 & 0 & (C_{11} - C_{12})/2 \end{pmatrix} \quad (2)$$

The calculated two independent elastic constants $C_{11}=18.40 \text{ Nm}^{-1}$ and $C_{12}=5.01 \text{ Nm}^{-1}$, which meet the Born criteria of mechanical stability²⁹: $C_{11} > 0$ and $C_{11} - C_{12} > 0$, confirming its mechanical stability. The shear modulus G^{2D} equals to $C_{66}=(C_{11}-C_{12})/2$ (6.70 Nm^{-1}). We calculate the direction-dependent Young's modulus $C_{2D}(\theta)$ ³⁰:

$$C_{2D}(\theta) = \frac{C_{11}C_{22} - C_{12}^2}{C_{11}\sin^4\theta + A\sin^2\theta\cos^2\theta + C_{22}\cos^4\theta} \quad (3)$$

where $A = (C_{11}C_{22} - C_{12}^2)/C_{66} - 2C_{12}$. Calculated results show that the RbKNaBi is mechanically isotropic due to $P3m1$ symmetry. The C_{2D} of RbKNaBi is 17.04 Nm^{-1} , which is between ones of K_2NaBi (18.83 Nm^{-1}) and Rb_2NaBi (16.44 Nm^{-1})¹⁶. The RbKNaBi monolayer demonstrates larger mechanical flexibility

than those of other well-known 2D materials (graphene and MoS_2)^{31,32}. It is found that the Poisson's ratio $\nu_{2D}(\theta)$ is independent of direction, and can be simply expressed as:

$$\nu_{2D} = \frac{C_{12}}{C_{11}} \quad (4)$$

The calculated ν_{2D} is 0.272.

Intrinsic polar electric field is responsible for the emergence of out-of-plane piezoelectricity and Rashba effect. The difference in atomic size and electronegativity of K and Rb atoms leads to inequivalent Bi-K and Bi-Rb bond lengths (3.727 and 3.855 \AA), and K-Bi-K and Rb-Bi-Rb bond angles (97.12 and 92.90°), giving rise to a net electric field pointing from the K layer to the Rb layer. To identify the inherent electric field further, the planar average of the electrostatic potential energy is plotted in Figure 2. The mirror asymmetry produces an electrostatic potential gradient ($\Delta\Phi$) of about 0.29 eV , which is related to the work function change of the structure. The magnitude of the net vertical electric field is estimated to be 0.20 eV/\AA , which is determined by the slope of the plane-averaged electrostatic potential between K and Rb atoms' minima. The predicted net vertical electric field is smaller than that of Janus MoSSe (0.856 eV/\AA)¹⁴, implying a weak vertical polarization. The small built-in electric field makes for switching Rashba spin-splitting by reversing electric-field direction.

IV. ELECTRONIC STRUCTURES AND ELECTRIC FIELD EFFECTS

Monolayer K_2NaBi and Rb_2NaBi are predicted are large-gap QSHIs¹⁶. The nontrivial topological properties may be broken by building Janus structure from a QSHI, for example Janus SrAlGaSe_4 and MoSSe as derivatives of QSHIs SrGa_2Se_4 and $1T'\text{-MoS}_2$ ^{33,34}. Next, we inves-

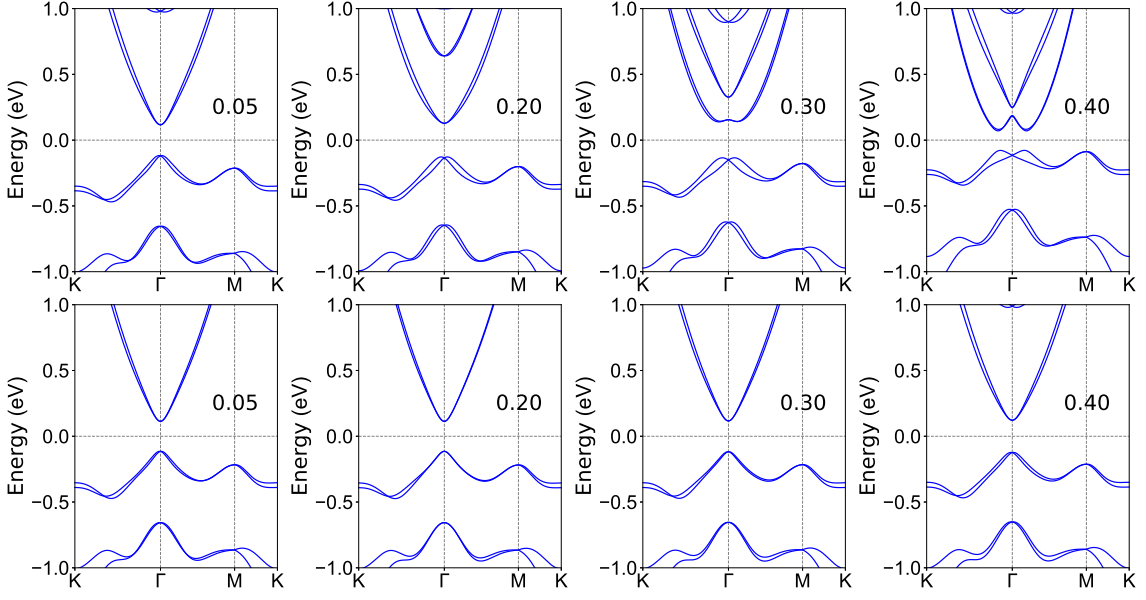


FIG. 6. (Color online) For RbKNaBi monolayer, the GGA+SOC energy band structures at representative $E=0.05, 0.20, 0.30$ and 0.40 V/Å with positive (Top plate) and negative (Bottom plate) electric field.

TABLE I. For monolayer K_2NaBi , $RbKNaBi$ and Rb_2NaBi , the elastic constants C_{ij} (Nm $^{-1}$), piezoelectric stress coefficient e_{ij} along with electronic part e_{ije} and ionic part e_{iji} (10^{-10} C/m), and piezoelectric strain coefficient d_{ij} (pm/V).

Name	C_{11}	C_{12}	e_{11e}	e_{11i}	e_{11}	e_{31e}	e_{31i}	e_{31}	d_{11}	d_{31}
K_2NaBi	19.46	5.29	0.15	0.66	0.81	—	—	—	5.69	—
$RbKNaBi$	18.41	5.02	0.23	0.51	0.74	-0.071	-0.024	-0.095	5.52	-0.41
Rb_2NaBi	17.08	4.51	0.293	0.348	0.641	—	—	—	5.10	—

tigate the electronic properties of RbKNaBi from GGA and GGA+SOC, and the Bi- s , $p_x + p_y$ and p_z projected band structures are plotted in [Figure 3](#). The GGA results show that RbKNaBi has a direct band gap of 0.110 eV with valence band maximum (VBM) and conduction band minimum (CBM) at the Γ point. However, the GGA+SOC results show an indirect band gap of 0.229 eV, and the VBM has a slight deviation from the Γ point. The calculated gap within SOC is close to those of K_2NaBi (0.18 eV) and Rb_2NaBi (0.22 eV)¹⁶. Without considering SOC, Bi- $p_x + p_y$ orbitals contribute to the VBM, while the CBM is dominated by Bi- s states. When including SOC, an inversion of Bi- s and Bi- $p_x + p_y$ states can be observed in the band structures, suggesting that monolayer RbKNaBi is a QSHI. On the other hand, the SOC can lift the degenerate spins due to relativistic effects. For Janus structures, the mirror asymmetry can produce built-in electric field, leading to Rashba spin-splitting (see [Figure 4](#)). The strength of the Rashba effect can be quantized by the Rashba energy (E_R) and Rashba constant (α_R), and the $\alpha_R = 2E_R/k_o$ with k_o for the Rashba momentum (see FIG.1 of electronic supplementary information (ESI)). The calculated $E_R=1.3$ meV and $\alpha_R=0.274$ eVÅ.

To further confirm nontrivial topological properties of

RbKNaBi, we calculate the Z_2 topological invariant. For a material with inversion symmetry, we can calculate Z_2 topological invariant by the product of parities of all occupied states at four time-reversal-invariant-momentum points in the 2D BZ. However, for RbKNaBi with broken spatial inversion symmetry, the Z_2 can be obtained by the calculation of Wannier charge center (WCC)³⁵. If Z_2 equals 1, a material is a topologically nontrivial, while $Z_2=0$ means trivial state. As plotted in [Figure 5](#) (a), the evolution lines of WCC cross an odd number of times by an arbitrary reference line, giving rise to $Z_2=1$, which indicates that monolayer RbKNaBi is a QSHI. The projected edge spectra along the $[100]$ direction is calculated, and the local density of states (LDOS) is shown in [Figure 5](#) (b). It is clearly seen that there is a single pair of helical edge states in the bulk bandgap. Remarkably, a sizeable bulk gap (229 meV) makes for observing the room-temperature quantum spin Hall (QSH) effect, because the large gap can stabilize the helical edge states against the interference of the thermally activated carriers.

A perpendicular electric field is used to explore the manipulation of the Rashba spin splitting of RbKNaBi. There are different atomic species on its upper and lower facets for Janus RbKNaBi, implying that applying $+z$

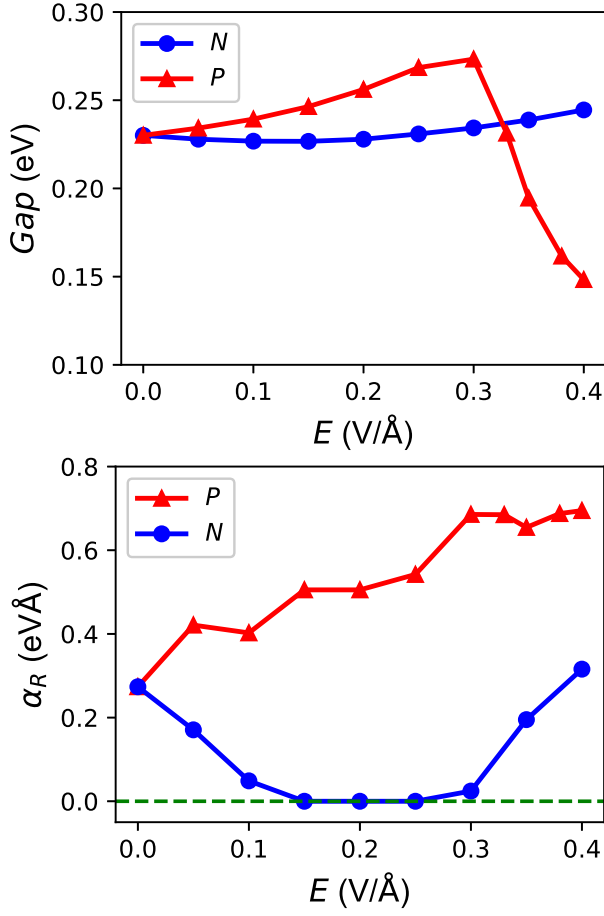


FIG. 7. (Color online) For RbKNaBi monolayer, the GGA+SOC gap and Rashba constant (α_R) as a function of electric field E with positive (P) and negative (N) electric field.

and $-z$ directional electric field are not equivalent. The energy band structures as a function of electric field E are calculated by using GGA+SOC. Some representative energy band structures are plotted in Figure 6, and the energy band gap vs E are shown in Figure 7. In considered positive E range, the gap firstly increases with increasing E , and then has a sudden drop at $E=0.30$ V/Å. However, the negative E has small effects on gap. In considered both positive and negative E ranges, the RbKNaBi is always a QSHI, and the calculated WCC evolutions at representative positive and negative $E=0.20$ V/Å are plotted in FIG.2 of ESI.

Next, we mainly investigate electric field effects on Rashba spin splitting of RbKNaBi. The calculated E_R as a function of both positive and negative E are presented in FIG.3 of ESI. For positive case, the E_R increases with increasing E . However, for negative situation, the E_R firstly decreases with increasing E , and become almost zero in a certain E region, and then increases. This is due to a competition between the external electric field and internal electric field. To clearly see the disappeared Rashba spin splitting, the enlarged valence bands cen-

tered at the Γ point near the Fermi level at representative positive and negative $E=0.20$ V/Å are plotted in FIG.4 of ESI. The calculated α_R vs E along both positive and negative directions are presented in Figure 7. The overall trend of α_R vs R is consistent with that of E_R vs E . It is clearly seen that the Rashba spin splitting of RbKNaBi is nonexistent, when E is between negative 0.15 V/Å and 0.25 V/Å. In this region, the Rashba spin splitting will be opened by reversing electric field direction (from negative E to positive E). This switch operation can expand the range of possible applications in future spintronic technology.

Besides, the constant energy (at an energy surface 0.16 eV below the Fermi level) spin-resolved 2D contours for the spin texture centered at the Γ point are plotted in Figure 8 under both positive and negative $E=0.2$ eV/Å. For positive case, the S_y components have a 90° of rotation as compared to S_x counterpart. The concentric spin-texture circles mean the purely 2D Rashba spin-splitting (an isotropic splitting). Only in-plane S_x and S_y spin components are present in the Rashba spin-splitting bands, while the out-of-plane S_z component is non-existent, which further confirms that the spin splitting under positive $E=0.2$ eV/Å has an isotropic 2D Rashba nature. For negative situation, no Rashba spin-splitting bands can be observed. Only out-of-plane S_z spin component is present, while in-plane S_x and S_y components vanish. It is clearly seen that the out-of-plane S_z spin component has three-fold rotational symmetry.

V. PIEZOELECTRIC PROPERTIES

When a strain or stress is applied on a non-centrosymmetric material, the electric dipole moments can be induced and produce electricity, called piezoelectric effect. The piezoelectric response of a material can be described by third-rank piezoelectric stress tensor e_{ijk} and strain tensor d_{ijk} . The relaxed piezoelectric tensors (e_{ijk} and d_{ijk}) include the ionic and electronic contributions:

$$e_{ijk} = \frac{\partial P_i}{\partial \varepsilon_{jk}} = e_{ijk}^{elc} + e_{ijk}^{ion} \quad (5)$$

and

$$d_{ijk} = \frac{\partial P_i}{\partial \sigma_{jk}} = d_{ijk}^{elc} + d_{ijk}^{ion} \quad (6)$$

in which P_i , ε_{jk} and σ_{jk} are polarization vector, strain and stress, respectively, and the superscripts *elc* and *ion* is used to denote electronic and ionic contributions. The e_{ijk}^{elc} and d_{ijk}^{elc} are also called clamped-ion piezoelectric coefficients, while e_{ijk} and d_{ijk} mean relax-ion cases. The e_{ijk} is related with d_{ijk} by elastic tensor C_{mnjk} :

$$e_{ijk} = \frac{\partial P_i}{\partial \varepsilon_{jk}} = \frac{\partial P_i}{\partial \sigma_{mn}} \cdot \frac{\partial \sigma_{mn}}{\partial \varepsilon_{jk}} = d_{imn} C_{mnjk} \quad (7)$$

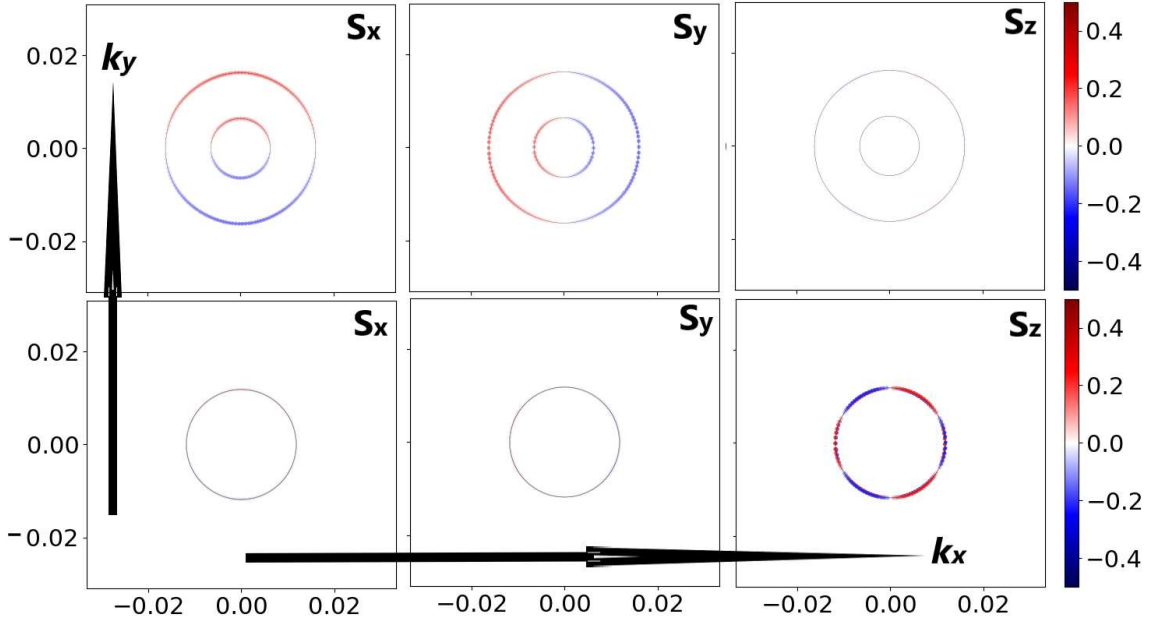


FIG. 8. (Color online) For RbKNaBi monolayer, the spin projected constant energy contour plots of spin texture calculated in a k_x - k_y plane centered at the Γ point at an energy surface 0.16 eV below the Fermi level with positive (Top plate) and negative (Bottom plate) electric field $E=0.20$ V/Å. In the color scale, red means spin-up states while blue means spin-down states.

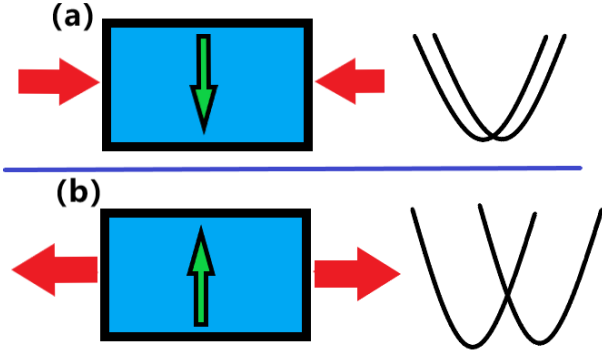


FIG. 9. (Color online) Schematic of biaxial in-plane strain tuned Rashba spin-splitting: the red arrows represent strain, while the green arrows represent electric field induced by piezoelectric effect; (a) the compressive strain induce negative electric field, which can reduce Rashba spin-splitting. (b) the tensile strain induce positive electric field, which can enhance Rashba spin-splitting.

With respect to K_2NaBi and Rb_2NaBi , for RbKNaBi, the introduction of Janus structure results in a lower degree of C_{3v} symmetry, and both the in-plane and out-of-plane piezoelectric effects are allowed, when a uniaxial in-plane strain is applied. By using Voigt notation, the 2D piezoelectric stress and strain tensors can be expressed as^{36,37}:

$$e = \begin{pmatrix} e_{11} & -e_{11} & 0 \\ 0 & 0 & -e_{11} \\ e_{31} & e_{31} & 0 \end{pmatrix} \quad (8)$$

$$d = \begin{pmatrix} d_{11} & -d_{11} & 0 \\ 0 & 0 & -2d_{11} \\ d_{31} & d_{31} & 0 \end{pmatrix} \quad (9)$$

It is found that only out-of-plane piezoelectric response can exist ($e_{11}/d_{11}=0$, but $e_{31}/d_{31} \neq 0$), when applying a biaxial in-plane strain. In other words, the pure out-of-plane piezoelectric response can be realized by imposed biaxial strain. Here, the two independent d_{11} and d_{31} can be derived by $e_{ik} = d_{ij}C_{jk}$:

$$d_{11} = \frac{e_{11}}{C_{11} - C_{12}} \quad \text{and} \quad d_{31} = \frac{e_{31}}{C_{11} + C_{12}} \quad (10)$$

We use the orthorhombic supercell (see Figure 1 (b)) to calculate the e_{11}/e_{31} of RbKNaBi. The predicted e_{11}/e_{31} is $0.74 \times 10^{-10} / -0.095 \times 10^{-10}$ C/m with ionic part $0.51 \times 10^{-10} / -0.024 \times 10^{-10}$ C/m and electronic part $0.23 \times 10^{-10} / -0.071 \times 10^{-10}$ C/m. For both e_{11} and e_{31} , the electronic and ionic parts have superposed contributions. Based on Equation 10, the predicted d_{11}/d_{31} is 5.52/-0.41 pm/V. The predicted d_{11} and d_{31} (absolute value) are higher than or compared with those of familiar 2D materials^{36,37}. The E along z direction can also be induced with a biaxial in-plane strain by piezoelectric effect, and then tune Rashba spin-splitting of RbKNaBi. When an in-plane vibration is applied to RbKNaBi, the Rashba effect will be modulated periodically. As shown in Figure 9 (a), the compressive strain induce negative electric field, which can reduce Rashba spin-splitting. However, Figure 9 (b) shows that the tensile strain in-

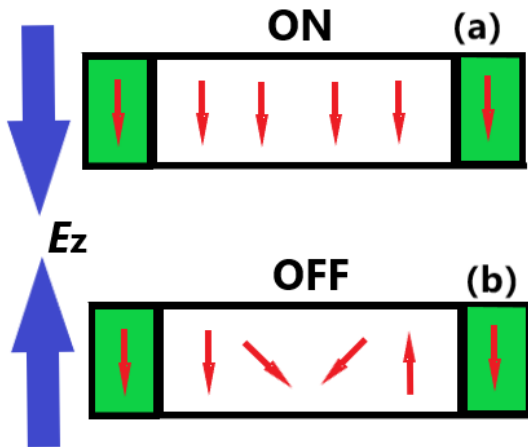


FIG. 10. (Color online) Schematic of spintronic devices: the red arrows represent spin, while the blue arrows represent electric field.

duce positive electric field, which can enhance Rashba spin-splitting.

The monolayer K_2NaBi and Rb_2NaBi possess horizontal mirror symmetry, and only in-plane d_{11} can exist, when a uniaxial in-plane strain is applied. For comparison, we also calculate the piezoelectric coefficients of K_2NaBi and Rb_2NaBi , and the related data are listed in Table I. It is found that the d_{11} of the three monolayers are very close, and the d_{11} of $RbKNaBi$ monolayer fall in between those of the K_2NaBi and Rb_2NaBi monolayers, as expected. The coexistence of piezoelectricity and nontrivial topological insulating phase, namely piezoelectric quantum spin Hall insulator (PQSHI), has potential advantages toward the development of high-speed and dissipationless electronic devices. Combining their nontrivial electronic structures, K_2NaBi , Rb_2NaBi and $RbKNaBi$ all are PQSHIs.

VI. DISCUSSION AND CONCLUSION

Some suggestions on experimental synthesis aspects of $RbKNaBi$ are discussed. Firstly, the dynamically stable bulk compounds K_2NaBi and Rb_2NaBi are ther-

modynamically stable against disproportionation into the competing phases³⁸. Secondly, by exfoliating these Na_3Bi -like alkali bismide three-dimensional Dirac semimetals K_2NaBi and Rb_2NaBi , their monolayer structures are also dynamically, thermally and mechanically stable¹⁶. Finally, similar to Janus monolayer MoS_2 from MoS_2 ^{12,13}, the $RbKNaBi$ can be synthesized experimentally with similar experimental techniques based on K_2NaBi or Rb_2NaBi monolayer.

The SOC effects (Rashba spin-splitting) can be reversibly turned on and off by reversing electric-field direction, which provides a high-speed switch for the subsequent development of spin devices to control the passage of electrons (see Figure 10). For example, two ferromagnetic electrodes in the same direction are set for the component. With an appropriate negative applied electric field, the injected electrons pass through the $RbKNaBi$ channel at a high speed and keep the spin orientation unchanged (Figure 10 (a)). When the external electric field direction is reversed, the spin of electrons in the channel will rotate under the effect of SOC, and will be blocked by the derived electrode (Figure 10 (b)). This possible spintronic device realizes the function of spintronic switch.

In summary, we have demonstrated that Rashba spin-splitting can be reversibly turned on and off by reversing electric-field direction in $RbKNaBi$. Calculated results show that the E_R and α_R are increased by the positive E , while a negative E suppresses the Rashba splitting to disappear, and then appears again. In a certain electric field region, simply reversing electric-field direction can achieve switching Rashba spin-splitting. Besides, it is proved that $RbKNaBi$ is a QSHI and possesses excellent piezoelectric properties, which makes $RbKNaBi$ become a multifunctional 2D material. Our findings can inspire more works about electric field-tuned switch of Rashba spin-splitting.

ACKNOWLEDGMENTS

This work is supported by Natural Science Basis Research Plan in Shaanxi Province of China (2021JM-456). We are grateful to Shanxi Supercomputing Center of China, and the calculations were performed on TianHe-2.

- ¹ J. J. Chen, K. Wu, W. Hu and J. L. Yang, *J. Phys. Chem. Lett.* **12**, 12256 (2021).
- ² G. Dresselhaus, *Phys. Rev.* **100**, 580 (1955).
- ³ Y. A. Bychkov and E. I. Rashba, *JETP Lett.* **39**, 78 (1984).
- ⁴ J. Nitta, T. Akazaki, T. H. Takayanagi and T. Enoki, *Phys. Rev. Lett.* **78**, 1335 (1997).
- ⁵ S. Singh and A. H. Romero, *Phys. Rev. B* **95**, 165444 (2017).
- ⁶ K. Wu, J. Chen, H. Ma, L. Wan, W. Hu, and J. Yang, *Nano Lett.* **21**, 740 (2021).
- ⁷ Y. Ma, Y. Dai, W. Wei, X. Li and B. Huang, *Phys. Chem.*

Chem. Phys. **16**, 17603 (2014).

- ⁸ H. L. Zhuang, V. R. Cooper, H. Xu, P. Ganesh, R. G. Hennig, P. Kent, *Phys. Rev. B* **92**, 115302 (2015).
- ⁹ C. Liu, H. Gao, Y. Li, K. Wang, L. A. Burton and W. J. Ren, *Mater. Chem. C* **8**, 5143 (2020).
- ¹⁰ L. Zhu, T. Zhang, G. Chen and H. Chen, *Phys. Chem. Chem. Phys.* **20**, 30133 (2018).
- ¹¹ D. Domaretskiy, M. Philippi, M. Gibertini, N. Ubrig, I. Gutiérrez-Lezama and A. F. Morpurgo, *Nat. Nanotechnol.* (2022). <https://doi.org/10.1038/s41565-022-01183-4>
- ¹² J. Zhang, S. Jia, I. Kholmanov, L. Dong, D. Er, W. Chen,

- H. Guo, Z. Jin, V. B. Shenoy, L. Shi and J. Lou, *ACS Nano* **11**, 8192 (2017).
- ¹³ A.-Y. Lu, H. Zhu, J. Xiao, C.-P. Chuu, Y. Han, M.-H. Chiu, C.-C. Cheng, C.-W. Yang, K.-H. Wei, Y. Yang, Y. Wang, D. Sokaras, D. Nordlund, P. Yang, D. A. Muller, M.-Y. Chou, X. Zhang and L.-J. Li, *Nat. Nanotechnol.* **12**, 744 (2017).
 - ¹⁴ Y. Chen, J. Y. Liu, J. B. Yu, Y. G. Guo and Q. Sun, *Phys. Chem. Chem. Phys.* **21**, 1207 (2019).
 - ¹⁵ T. Hu, F. H. Jia, G. D. Zhao, J. Y. Wu, A. Stroppa and W. Ren, *Phys. Rev. B* **97**, 235404 (2018).
 - ¹⁶ J. W. Jiang, X. Q. Guo, Z. Ma, G. Wang, Y. G. Xu and X. W. Zhang, *J. Mater. Chem. C* **10**, 11329 (2022).
 - ¹⁷ P. Hohenberg and W. Kohn, *Phys. Rev.* **136**, B864 (1964); W. Kohn and L. J. Sham, *Phys. Rev.* **140**, A1133 (1965).
 - ¹⁸ G. Kresse, *J. Non-Cryst. Solids* **193**, 222 (1995).
 - ¹⁹ G. Kresse and J. Furthmüller, *Comput. Mater. Sci.* **6**, **15** (1996).
 - ²⁰ G. Kresse and D. Joubert, *Phys. Rev. B* **59**, 1758 (1999).
 - ²¹ J. P. Perdew, K. Burke and M. Ernzerhof, *Phys. Rev. Lett.* **77**, 3865 (1996).
 - ²² A. Togo, F. Oba, and I. Tanaka, *Phys. Rev. B* **78**, 134106 (2008).
 - ²³ X. Wu, D. Vanderbilt and D. R. Hamann, *Phys. Rev. B* **72**, 035105 (2005).
 - ²⁴ Q. Wu, S. Zhang, H. F. Song, M. Troyer and A. A. Soluyanov, *Comput. Phys. Commun.* **224**, 405 (2018).
 - ²⁵ A. A. Mostofia, J. R. Yatesb, G. Pizzif, Y.-S. Lee, I. Souza, D. Vanderbilt and N. Marzari, *Comput. Phys. Commun.* **185**, 2309 (2014).
 - ²⁶ U. Herath, P. Tavadze, X. He, E. Bousquet, S. Singh, F. Munoz and A. H. Romero, *Computer Physics Communications* **251**, 107080 (2020).
 - ²⁷ E. Mariani and F. V. Oppen, *Phys. Rev. Lett.* **100**, 076801 (2008).
 - ²⁸ J. Carrete, W. Li, L. Lindsay, D. A. Broido, L. J. Gallego and N. Mingo, *Mater. Res. Lett.* **4**, 204 (2016).
 - ²⁹ R. C. Andrew, R. E. Mapasha, A. M. Ukpong and N. Chetty, *Phys. Rev. B* **85**, 125428 (2012).
 - ³⁰ E. Cadelano, P. L. Palla, S. Giordano and L. Colombo, *Phys. Rev. B* **82**, 235414 (2010).
 - ³¹ K. N. Duerloo, M. T. Ong and E. J. Reed, *J. Phys. Chem. Lett.* **3**, 2871 (2012).
 - ³² C. Lee, X. g Wei, J. W. Kysar and J. Hone, *Science* **321**, 385 (2008).
 - ³³ S. D. Guo, Y. T. Zhu, W. Q. Mu and X. Q. Chen, *J. Mater. Chem. C* **9**, 7465 (2021).
 - ³⁴ H. W. Xu, H. Wang, J. Zhou, Y. F. Guo, J. Kong and J. Li, *npj Computational Materials* **7**, 31 (2021).
 - ³⁵ A. A. Soluyanov and D. Vanderbilt, *Phys. Rev. B* **83**, 235401 (2011).
 - ³⁶ M. N. Blonsky, H. L. Zhuang, A. K. Singh and R. G. Hennig, *ACS Nano*, **9**, 9885 (2015).
 - ³⁷ L. Dong, J. Lou and V. B. Shenoy, *ACS Nano*, **11**, 8242 (2017).
 - ³⁸ X. Chen, W. Chen, S. Yu, S. Xu, X. Rong, P. Huang, X. Zhang and S. H. Wei, *J. Mater. Chem. C* **8**, 1257 (2020).